AGU PUBLICATIONS

JGR

Journal of Geophysical Research: Oceans

RESEARCH ARTICLE

10.1002/2016JC011851

Special Section:
Oceanic Responses and Feedbacks to Tropical Cyclones

A genesis potential index for Western North Pacific tropical cyclones by using oceanic parameters

Min Zhang[1], Lei Zhou[2], Dake Chen[2], and Chunzai Wang[3,4]

[1]Key Laboratory of Coastal Disaster and Defence, Hohai University, Nanjing, China, [2]State Key Laboratory of Satellite Ocean Environment Dynamics, Second Institute of Oceanography, SOA, Hangzhou, China, [3]State Key Laboratory of Tropical Oceanography, South China Sea Institute of Oceanology, Chinese Academy of Sciences, Guangzhou, China, [4]Physical Oceanography Laboratory/Qingdao Collaborative Innovation Center for Marine Science and Technology, Ocean University of China, Qingdao, China

Key Points:
- A new genesis potential index for tropical cyclone is created by explicitly considering the oceanic parameters
- The new genesis potential index has a comparable ability to represent the statistics of tropical cyclone genesis
- The new index is useful for evaluating the influence of inner ocean variabilities on TC genesis, in the context of climate change

Correspondence to:
L. Zhou,
lzhou@sio.org.cn

Citation:
Zhang, M., L. Zhou, D. Chen, and C. Wang (2016), A genesis potential index for Western North Pacific tropical cyclones by using oceanic parameters, *J. Geophys. Res. Oceans*, *121*, 7176–7191, doi:10.1002/2016JC011851.

Received 31 MAR 2016
Accepted 2 SEP 2016
Accepted article online 7 SEP 2016
Published online 30 SEP 2016

© 2016. American Geophysical Union. All Rights Reserved.

Abstract This study attempts to create a tropical cyclone (TC) genesis potential index (GPI) by considering oceanic parameters and necessary atmospheric parameters. Based on the general understanding of the oceanic impacts on TC genesis, many candidate factors are evaluated and discriminated, resulting in a new GPI index, which is referred to as GPI_{ocean}. GPI_{ocean} includes the parameters of (1) absolute vorticity at 1000 hPa, (2) net sea surface longwave radiation, (3) mean ocean temperature in the upper mixed layer, and (4) depth of the 26°C isotherm. GPI_{ocean} is comparable to existing GPIs in representing TC genesis over the western North Pacific on seasonal and interannual variations. The same procedure can be applied to create a similar GPI for the other ocean basins. In the context of climate change, this new index is expected to be useful for evaluating the oceanic influences on TC genesis by using ocean reanalysis products and climate model outputs.

1. Introduction

About two dozens of tropical cyclones (TCs) are generated over the western North Pacific every year. TC genesis has pronounced seasonal and interannual variabilities, which are attributable to the atmospheric and oceanic environments. A lot of studies have been conducted over the western North Pacific. For example, *Chan et al.* [2004] found that the interannual typhoon activities appeared to be largely controlled by the large-scale atmospheric factors. In this region, TC genesis is modulated by many environmental factors, such as the Paci?c meridional mode [*Zhang et al.*, 2016] and the position of the tropical upper tropospheric trough [*Wang and Wu*, 2016; *Wu et al.*, 2015]. *Yu et al.* [2016] showed that the variabilities of TC genesis number were consistent with the first SST mode over the tropical North Pacific. Thus, the relationship between the statistical properties of TC genesis and the large-scale climate factors is an interesting problem of scientific and social importance, especially in the context of climate change.

Many studies have been conducted to address this problem. *Gray* [1979] was a pioneer to represent the seasonal and spatial features of TCs with key environmental parameters. *Royer et al.* [1998] used the convective potential, instead of sea surface temperature (SST), as the threshold in the Convective Yearly Genesis Potential (CYGP) index. Then, incorporating the cyclone dynamics and the classical theory of Carnot cycle, *Emanuel and Nolan* [2004] developed another genesis potential index (GPI; referred to as GPI04 hereafter), which had an explicit dependence on the potential intensity (PI) of TCs [*Emanuel*, 1997], the low-troposphere wind velocity, relative humidity, and the vertical wind shear. GPI04 has been widely used, but it may not reproduce the projected future changes in the TC genesis frequency counted directly from model outputs [*Yokoi et al.*, 2009]. The vertical velocity, which was expected to play an important role in TC genesis, was not included in GPI04, although its effect was partly taken into account with the relative humidity at the midtroposphere. The importance of the vertical velocity on the TC genesis frequency was discussed by *Zhao and Held* [2012]. *Murakami and Wang* [2010] adopted the vertical velocity in their GPI (referred to as GPI10 hereafter), showing that their GPI had a better performance than GPI04 over the eastern Pacific Ocean and the tropical Atlantic Ocean. Moreover, *Emanuel* [2010] created a new GPI by replacing the midlevel relative humidity with the moist entropy deficit. *Tippett et al.* [2011] adopted relative SST and proposed a Poisson regression index. *Bruyère et al.* [2012] simplified GPI04 by only using the PI and the vertical shear. All above statistical GPIs facilitate the

studies of the environmental impacts on TC genesis, which usually use low-resolution reanalysis products, atmosphere-only models, and atmosphere-ocean coupled models [such as *Camargo et al*., 2007b; *Emanuel*, 2005; *Vecchi and Soden*, 2007a,2007b; *Vincent et al*., 2011; *Yokoi et al*., 2009, and many others].

So far, most factors in existing GPIs are atmospheric factors. The oceanic impact is usually grossly denoted with the SST (or other very similar variables) in the term of PI. However, in reality, the SST is not the only oceanic property that can leave fingerprints on TC genesis. Actually, both observations and model simulations indicate that the local SST may not play a critical role in TC genesis. Different oceanic properties such as the subsurface ocean structure can have different statistical relations with TC genesis. Therefore, we intend to create a new GPI by explicitly adopting necessary oceanic factors. The new GPI is expected to have a comparable ability to represent TC genesis.

Although a quantitative and ubiquitous theory about the oceanic influence on TC genesis is still missing, many oceanic properties have been shown to have a close relation with TCs. As mentioned above, the SST has been included in some established GPIs, denoting the energy source of TC genesis. *Gray* [1979] used the SST of 26°C as a threshold, but it was replaced by the relative temperature with respective to the TC outflow temperature [*Emanuel*, 1995, 1997]. Since strong winds during TCs can effectively disturb the upper ocean layer, the thermodynamics below the ocean surface also have impacts on TCs and the subsurface contribution to TCs is regarded as a key to improve the TC index. For example, *Lin et al*. [2013] proposed to replace the SST with the mean temperature in the precyclone upper ocean mixed layer in the PI index. Except for the local thermal structure, the remote high SST can stabilize the local atmosphere via downdraft, influencing the long-term variability of TCs. Accordingly, *Vecchi and Soden* [2007a] proposed to use the difference between the local SST and the tropical zonal mean SST in the PI index for TCs. Besides, the surface heat flux, the upper ocean heat content (OHC), the mixed layer depth, the temperature difference between the sea surface and the bottom of the mixed layer, and the lapse rate of the upper thermocline are all shown to have influences on TCs [*Black et al*., 2007; *Price*, 2009; *Scoccimarro et al*., 2011; *Shay et al*., 2000; *Wu et al*., 2007]. Overall, various oceanic properties have been found to have significant impacts on both TC genesis and intensity. Hence, we use all above properties as candidates for the new GPI. After the candidate factors are assumed based on the physical understandings, a stepwise regression method and statistical tests are applied to select the factors that can significantly contribute to the index. Finally, a new GPI adopting oceanic parameters are created. Note that not all parameters in the new GPI are oceanic parameters and the reason will be discussed in the last section. It is shown that the new GPI has a comparable ability to represent TC genesis over the western North Pacific.

This paper is organized as follows. Data and methods are described in section 2. In section 3, the GPI explicitly involving oceanic parameters is created and its ability to represent TC genesis is assessed by comparing with the existing GPIs. The performances of the new GPI on seasonal and interannual scales are analyzed in section 4. Conclusions and discussion are presented in section 5.

2. Data and Methods

2.1. Data

All atmospheric variables, such as wind velocity, relative humidity, and vertical pressure velocity, are obtained from the monthly National Center for Environmental Prediction/National Center for Atmospheric Research (NCEP/NCAR) [*Kalnay et al*., 1996] reanalysis. Surface heat fluxes, including shortwave radiation, longwave radiation, latent heat flux, and sensible heat flux, are also obtained from the NCEP/NCAR reanalysis. The upward heat flux from the ocean to the atmosphere is defined positive. Monthly ERA-40 reanalysis [*Uppala et al*., 2005] from the European Centre for Medium-Range Weather Forecasts (ECMWF) are also used. Since the results are qualitatively the same as the ones using the NCEP/NCAR reanalysis, they are not shown. Monthly SSTs are obtained from the Met Office Hadley Center with a resolution of 1° latitude × 1° longitude [*Rayner et al*., 2003] and the ocean temperatures are the EN4 quality controlled ocean data (EN.4.0.2) from the Hadley Centre subsurface temperature and salinity objective analyses with a resolution of 1° latitude × 1° longitude [*Good et al*., 2013]. The locations and times of TC genesis are obtained from the best-track data set developed by the U.S. Joint Typhoon Warning Center (JTWC). In this study, a TC is generated when the maximum sustained wind speed reaches 17.5 m s^{-1} (34 knot) for the first time [*Park et al*., 2011]. The analysis period is from 1948 to 2012, which is the common period for all

data sets. The TC genesis data from Japan Meteorological Agency (JMA) and from China Meteorological Agency (CMA) are also used for calibration. Since they are similar to the JTWC TC genesis, the results are not explicitly shown.

2.2. Statistical Methods

Without a quantitative theory about the physical mechanism of the oceanic impacts on TC genesis, the empirical statistical methods are useful for selecting oceanic factors for the new GPI. The statistical methods used in this study are generally the same as the ones widely used previously, such as in *Camargo et al*. [2007b], *Emanuel and Nolan* [2004], *Lin et al*. [2013], *Murakami and Wang* [2010], and *Tippett et al*. [2011]. GPI04 developed by *Emanuel and Nolan* [2004] and GPI10 developed by *Murakami and Wang* [2010] are used as the control indices. The coefficients in these two indices are recalculated over the western North Pacific using the least square fitting, so that they have the highest consistency with observations in our research domain. In order to compare the effectiveness of any two GPIs, the differences of the correlation coefficients between each index and the observation can be tested with the two-tailed Hotelling's *t* square test [*Hotelling*, 1940]. Suppose two GPIs are denoted with GPI_1 (e.g., GPI04) and GPI_2 (e.g., GPI10), and their correlations with observations are r_{o1} and r_{o2}, respectively, where the subscript "o" denotes the observation. The correlation coefficient between the two indices is denoted with r_{12}. The following formula obeys the Hotelling's *t* square distribution,

$$t = (r_{o1} - r_{o2}) \frac{\sqrt{(n-3)(1+r_{12})}}{\sqrt{2\left(1 - r_{o1}^2 - r_{o2}^2 - r_{12}^2 + 2r_{o1}r_{o2}r_{12}\right)}} \tag{1}$$

where n is the number of records. If r_{o1} is significantly larger than r_{o2}, GPI_1 has a better consistency with the observations than GPI_2, and vice versa. If r_{o1} and r_{o2} have no significant difference, the two GPIs have a comparable ability to represent the observed TC genesis. Since the actual correlation coefficients may not be normally distributed, the *t* value in equation (1) may be overestimated, leading to a Type 1 error (incorrect rejection of a true null hypothesis). Hence, Steiger's *Z* test [*Steiger*, 1980] is also applied to test the significance of the difference between two correlation coefficients.

As briefly summarized in section 1, various factors representing the oceanic environment are selected as candidates. They are (1) the local SST, (2) the relative SST defined as the difference between the local SST and the mean tropical SST (zonal mean SST within 30°N–30°S), (3) the surface heat fluxes (including longwave radiation, shortwave radiation, latent heat flux, and sensible heat flux), (4) the mixed layer depth (defined in 12 ways; see details below), (5) the mean temperature in the upper mixed layer, (6) the temperature difference between the sea surface and the bottom of the mixed layer, (7) the upper OHC ($Q_{ohc} = \rho C_p \int_0^{MLD} T(z)dz$, where ρ is the sea water density, C_p is the heat capacity, and MLD denotes the mixed layer depth), (8) the depth of the isotherms at various temperatures, such as the 26°C isotherm (D_{26}), (9) the mean temperature above D_{26}, and (10) some common oceanic environmental parameters in the thermocline (such as the thermocline depth, the lapse rate at the thermocline, and the mean temperature in the upper thermocline depth). Note that the physical mechanism between TC genesis and a few candidates above (such as the local SST) may be controversial. But we intend to include as many potential candidates as possible, which guarantees the completeness of our analysis. Actually, the ones (such as the local SST) that have a loose connection with TC genesis are not selected into the new GPI by the statistical method, as the results will show in the following. When choosing the candidate parameters, we purposely pick up the common ones that are available in reanalysis products and climate model outputs, so that the result can facilitate the possible application of this new index. Some small-scale processes (such as the ocean waves, diapycnal mixing, and ocean spray) are not selected, although previous studies have indicated that they are able to have impacts on TCs. Then, a stepwise regression is applied to each parameter, following the method described in *Ballabrera-Poy et al*. [2002] and *Draper and Smith* [1998]. If the inclusion of a candidate factor can improve the ability of the new GPI (quantitatively determined using the Hotelling's *t* square test and the Steiger's *Z* test), the factor is selected. Otherwise, it is discarded. Although the selection of candidates is partially subjective, the regression method is objective and it provides a framework for the deterministic selection of the ocean parameters for the new index.

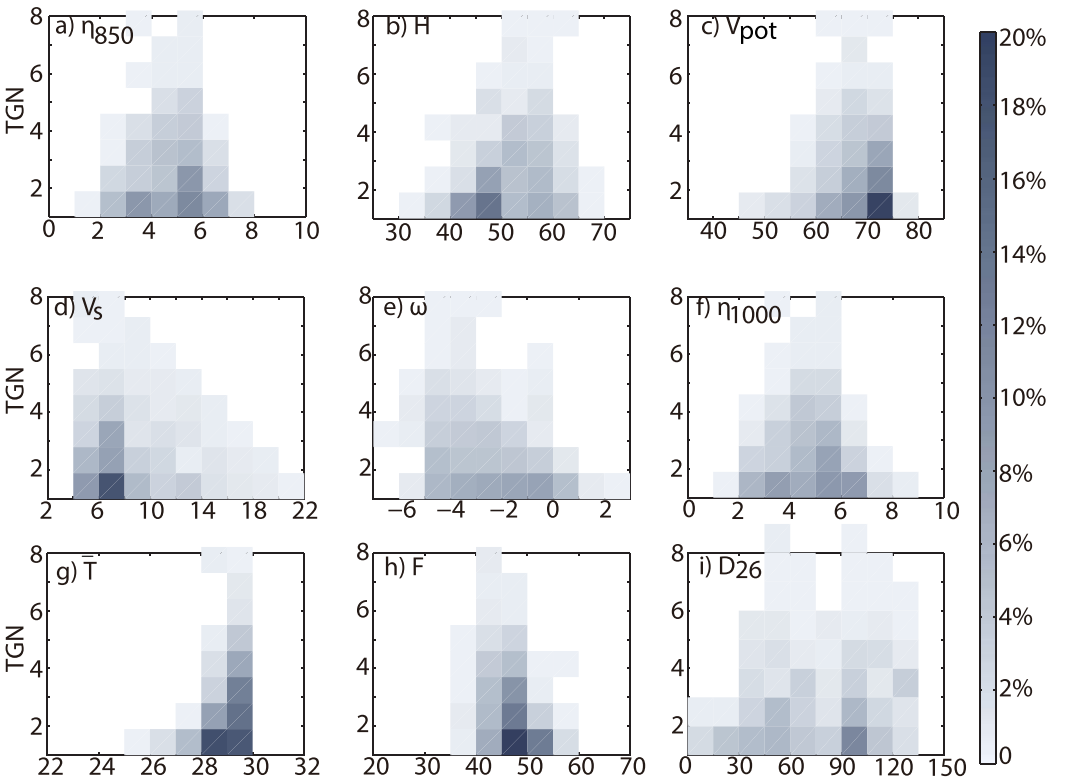

Figure 1. Joint probability distribution of the grid points with respect to the TC genesis number and different factors used in equations (2) and (3). TGN is short for TC genesis number. The $\boldsymbol{x}$ axis in each plot is (a) $\boldsymbol{\eta}_{850}$ in $10^{-5}\mathbf{s}^{-1}$; (b) H in percentage; (c) V_{pot} in m s^{-1}**;** (d) V_s in m s^{-1}; (e) ω in 10^{-2} Pa s^{-1}; (f) $\boldsymbol{\eta}_{1000}$ in $10^{-5}\mathbf{s}^{-1}$; (g) $\bar{\boldsymbol{T}}$ in °C; (h) F in W m^{-2}; (i) $D_{\mathbf{26}}$ in m.

3. A New TC GPI Over the Western North Pacific

3.1. GPI With Atmospheric Parameters

Generally, GPI04 and GPI10 have a good performance in representing TC genesis [*Menkes et al*., 2011], thus they are used as the control indices to calibrate the ability of the new GPI adopting oceanic parameters. The format of GPI10 is

$$\mathrm{GPI}=p|10^5\eta_{850}|^a\left(\frac{H}{50}\right)^b\left(\frac{V_{pot}}{70}\right)^c(1+0.1V_s)^d\left(\frac{-\omega+0.1}{0.1}\right)^e, \tag{2}$$

where η_{850} is the absolute vorticity at 850 hPa, H is the relative humidity at 700 hPa, V_{pot} is the PI, V_s is the wind shear between 850 and 200 hPa, and ω is the vertical pressure velocity at 500 hPa. The coefficient p enables GPI has the best least square fit with the observed TC genesis and $p = 0.07$ in GPI10. The format of GPI04 is similar, except that the vertical velocity (the last term in equation (2)) is not included. The joint probability distributions of the grid points with respect to the TC genesis number and each term on the right hand side of equation (2) over the western North Pacific (within 100°E–180°E and 0°N–40°N) are shown in Figures 1a–1e). Most TCs generate when η_{850} is on the order of 10^{-5} s^{-1}, H is around 50%, V_{pot} is around 70 m s^{-1}, V_s is on the order of 10 m s^{-1}. The amplitude of ω is always less than 0.1 Pa s^{-1}. Therefore, the normalized formats of all terms in equation (2) remain valid over the western North Pacific. In order to guarantee the best performance of the control indices, the coefficients *a–e* in equation (2) are reevaluated using the least square fitting and the results are listed in Table 1. For comparison, the original coefficients used in *Emanuel and Nolan* [2004] and *Murakami and Wang* [2010] are also listed in Table 1. The correlations between each GPI and observations are listed in Table 2, along with the *t* values for the Hotelling's *t* square test and the *z* values for the Steiger's *Z* test between every two GPIs. If the *t* value and the *z* value listed in Table 2 are larger than 1.96, the two corresponding GPIs have significantly different correlations with observations at a 95% confidence level. It can be seen that GPI10 has a significantly larger correlation with observations than GPI04 does.

Table 1. The Exponential Coefficients for Various GPIs

	a	*b*	*c*	*d*	*e*	*f*	*g*	*h*	*i*
GPI_{ocean}						0.9	7.64	−2.73	0.25
$GPI10_{WP}$	1.46	1.43	2	−0.39	2				
$GPI04_{WP}$	1.5	3	3	−0.3					
GPI10	1.5	3	3	−2	1				
GPI04	1.5	3	3	−2					

Therefore, as argued in *Murakami and Wang* [2010], the explicit inclusion of vertical velocity can improve the performance of GPI over the western North Pacific. The GPIs with recalculated coefficients over the western North Pacific are referred to as $GPI04_{WP}$ and $GPI10_{WP}$, corresponding to GPI04 and GPI10, respectively. It can be seen from Table 2 that the locally regressed GPIs have higher correlation coefficients with the observations, which confirms the necessity of the reevaluation in the local research domain [*Fu et al.*, 2012]. In addition, similar to the relation between GPI04 and GPI10, the inclusion of vertical velocity also improves the index's ability, since $GPI10_{WP}$ has a higher correlation with observations than $GPI04_{WP}$ does.

The differences between various GPIs can also be seen from their spatial distributions (Figure 2). In reality (Figure 2a), TCs mainly generate in two regions: one is over the northern South China Sea (SCS) and the other one is within 10°N–24°N and 120°E–150°E. Both GPI04 and GPI10 underestimate TC genesis over the northern SCS and the western Pacific. Meanwhile, they yield false genesis along the eastern coast of Vietnam and along the Kuroshio, since warm SSTs in these two regions lead to unrealistically high V_{pot} (not shown). The bias along the Kuroshio reduces a little in $GPI04_{WP}$ and $GPI10_{WP}$. However, the bias along the Vietnam coast becomes even worse in $GPI04_{WP}$. For $GPI10_{WP}$, the reconstructions over the northern SCS and over the western North Pacific are clearly better than the other indices, although the bias along the Vietnam coast remains similar to that in GPI10. In general, $GPI10_{WP}$ has the best performance in representing TC genesis over the western North Pacific. Thus, it is used as the major control to calibrate the new GPI adopting the oceanic parameters in the following discussion.

3.2. GPI With Oceanic Parameters Over the Western North Pacific

The candidate parameters are the ones listed in section 1, which have been shown to have noticeable impacts on TCs in previous studies. However, since TCs are a phenomenon in the atmosphere, it is not reasonable to surmise that the statistical properties of TC genesis can be captured without using any atmospheric parameters at all. Thus, we do not intend to exclude all atmospheric factors. However, considering the possible application of the new GPI (see detailed discussion in the last section), we intend to include the necessary atmospheric parameters at the sea surface and we purposely avoid all parameters at a pressure level above the sea surface (such as η_{850} in equation (2)).

With the stepwise regression method, four factors that can significantly improve the performance of the new index are finally selected. They are (1) the absolute vorticity at 1000 hPa (η_{1000}, not η_{850} used in equation (2)), (2) the mean temperature in the ocean upper mixed layer ($\bar{T}$; not the local SST), (3) the net longwave radiation (F) at the sea surface, and (4) the depth of the 26°C isotherm (D_{26}). The method to

Table 2. Spatial Correlations [$r(G(x, y), \mathrm{obs}(x, y))$] Between Each GPI and Observations[a]

t Value/*z* Value	GPI04 $r = 0.39$	GPI10 $r = 0.45$	$GPI04_{WP}$ $r = 0.50$	$GPI10_{WP}$ $r = 0.53$	GPI_{ocean} $r = 0.54$
GPI04 $r = 0.39$	Nan	5.03/4.87	3.78/3.70	4.60/4.47	3.86/3.76
GPI10 $r = 0.45$		Nan	2.03/2.01	3.48/3.43	2.59/2.55
$PI04_{WP}$ $r = 0.50$			Nan	2.26/2.24	**1.49/1.48**
$GPI10_{WP}$ $r = 0.53$				Nan	**0.24/0.24**
GPI_{ocean} $r = 0.54$					Nan

[a]All data are from 1948 to 2012. The *r* values under each GPI are the correlation coefficient between the GPI and observations. The number before (behind) the slash is the *t* statistic (*Z* statistic) of the correlations between two GPIs and the observations. When the *t* values and *z* values are larger than 1.96, the two GPIs have different correlations with observations at a confidence level of 95%. The bold numbers indicate insignificant differences between two GPIs at a confidence level of 95%.

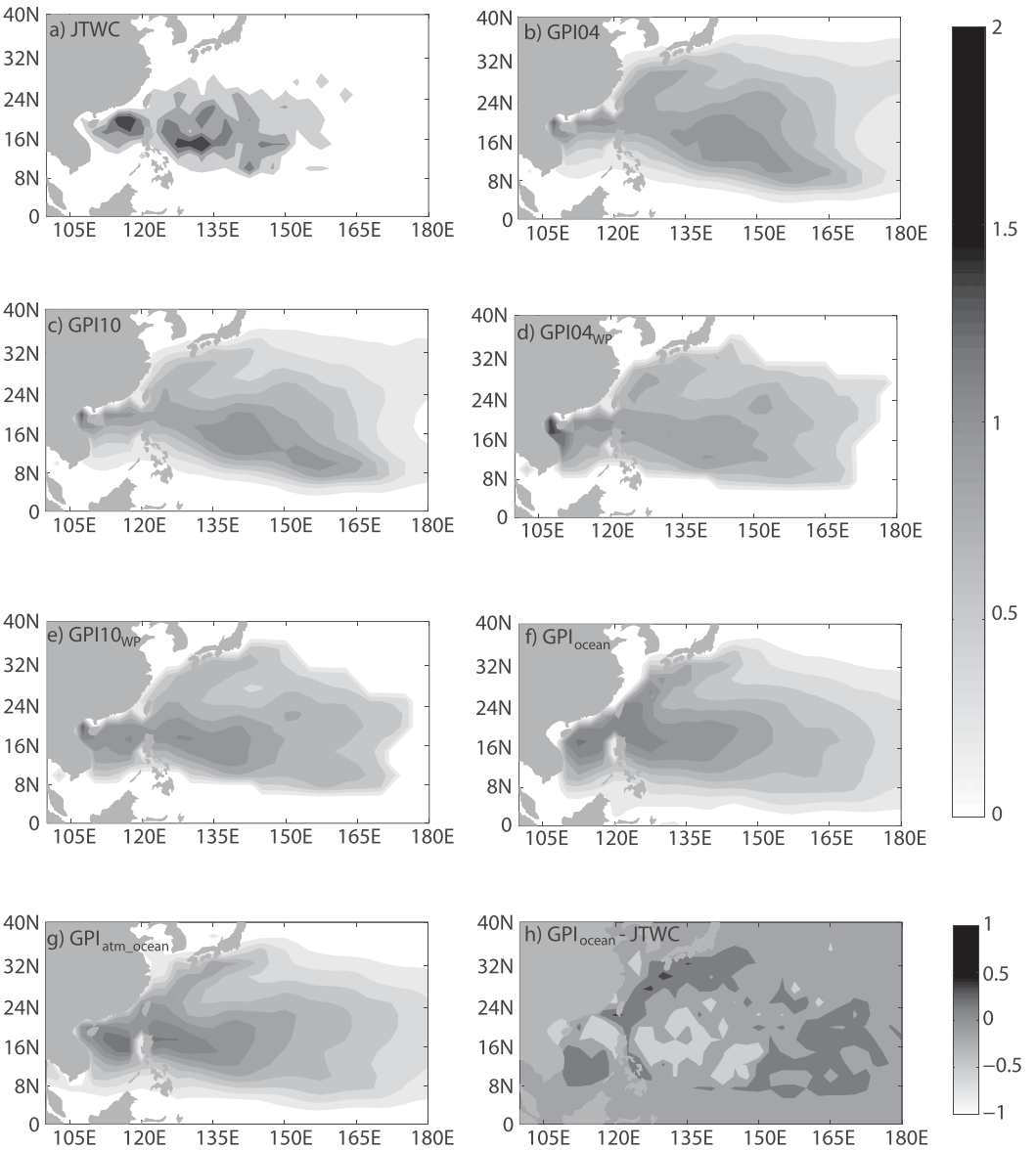

Figure 2. (a) Climatological mean TC genesis number from July to September, obtained from JTWC. (b–g) The same as Figure 2a, but obtained with different GPIs. (h) GPI$_{ocean}$—observations from JTWC.

Table 3. Methods to Determine the Mixed Layer Depth and Corresponding References[a]

Criterion/Method	Reference Depth	Reference
$\Delta T = 0.1°C$	10 m	*Sprintall and Roemmich* [1999]
$\Delta T = 0.2°C$	**5 m**	***Thompson*** **[1976]**
$\Delta T = 0.2°C$	10 m	*de Boyer Montégut et al.* [2004]
$\Delta T = 0.5°C$	5 m	*Silva et al.* [2009]
$\Delta T = 0.8°C$	5 m	*Chu et al.* [2010]
$\Delta T = 0.8°C$	10 m	*Kara et al.* [2000]
$\Delta T = 1°C$	5 m	*Lamb* [1984]
$\Delta T = 1°C$	10 m	*Rao et al.* [1989]
$\partial T/\partial z = 0.015°C/m$		*Defant* [1961]
$\partial T/\partial z = 0.025°C/m$		*Lukas and Lindstrom* [1991]
$\partial T/\partial z = 0.05°C/m$		*Chu et al.* [2002]
Maximum curvature		*Kara et al.* [2009]

[a]The one in bold is the method that is used for the analysis in this study.

determine the mixed layer depth is not unique and 12 methods (listed in Table 3) are tried. The results show no significant differences between different methods. Considering the possible application of the new index, the methods depending on the vertical gradient (the last four methods in Table 3) are not preferable because some ocean reanalysis products or ocean model outputs may not have a high vertical resolution to guarantee a reliable estimate of the vertical temperature gradient. In addition, the first layer in the EN4 ocean data is actually at 5 m

depth. Thus, in this study, the mixed layer depth is defined as the depth where the temperature is smaller than the temperature at 5 m depth by 0.2°C, following *Thompson* [1976].

For each candidate parameter, its possible format in the GPI is also determined based on its probability distribution with respect to the TC genesis numbers (Figures 1f–1i; only the probability distributions of the finally selected factors are shown). Therefore, although the format of each factor in the new GPI is not determined based on the physical mechanisms of the oceanic impacts on TC genesis, it is not arbitrarily chosen. The probability distribution of η_{1000} in Figure 1f is similar to the one of η_{850} in Figure 1a, i.e., TC tends to generate when η_{1000} is on the order of 10^{-5} s^{-1}. Thus, the format of η_{1000} in the new GPI remains the same as the format of η_{850} in equation (2). As shown in Figure 1g, most TCs generate when $\bar{T}$ is larger than 26°C (consistent with the criterion used by *Gray* [1979]) and the genesis number increases with $\bar{T}$. Thus, $\bar{T}$ is normalized by 26°C. In the context of climate change or global warming, $\bar{T}$ may change. But it is not necessary to modify the temperature (i.e., 26°C) used for the normalization, since it only makes the following regression process easier, but does not change the statistical relation between GPI and $\bar{T}$. The dependence of TC genesis on F is not monotonous (Figure 1h). Most TCs generate when F is between 35 W m^{-2} and 60 W m^{-2} (positive radiation is upward). Hence, F is normalized by 45 W m^{-2}. The dependence of TC genesis on D_{26} is largely uniform between 15 and 120 m. But there are two weak peaks in Figure 1i. One is between 35 and 65 m, which corresponds to TC genesis in the SCS. The other one is between 90 and 120 m, corresponding to TC genesis over the western North Pacific. In order to make a compromise between the two regions, D_{26} is normalized by 80 m, although TC genesis probability around this depth is not high. Overall, the format for the new GPI (referred to as GPI_{ocean} hereafter) is written as:

$$GPI_{ocean} = p|10^5 \eta_{1000}|^f \left(\frac{\bar{T}}{26}\right)^g \left(\frac{F}{45}\right)^h \left(\frac{D_{26}}{80}\right)^i, \quad (3)$$

where f, g, h, and i are coefficients determined with the method of least squares over the western North Pacific. The coefficient p enables the best least square fit between GPI_{ocean} and observations, and $p = 7.4 \times 10^{-3}$ in equation (3). The best fitting coefficients are listed in Table 1. The correlation coefficient between GPI_{ocean} and observations is 0.54. The t test and the Z test are applied to the correlation between GPI_{ocean} and observations, testing the significance of its difference from the correlations between the existing GPIs and observations (Table 2). One can see that GPI_{ocean} has a significantly higher correlation with observations than GPI04 and GPI10 do. The correlation coefficient of 0.54 is slightly higher than that of $GPI04_{WP}$ (0.50) and $GPI10_{WP}$ (0.53), but the differences are not statistically significant. The spatial distribution of GPI_{ocean} is shown in Figure 2f, and its differences from the observations are shown in Figure 2h. The bias along the Vietnam coast almost disappears in GPI_{ocean} and the TC genesis numbers over the northern SCS and western North Pacific are more consistent with observations (Figure 2a). However, the bias along the Kuroshio is still discernible, mainly due to the high $\bar{T}$ in that region (see details below). Therefore, considering the correlation and spatial consistency with observations, GPI_{ocean} has a comparable effectiveness with $GPI10_{WP}$ (the best existing index in this region) for representing TC genesis over the western North Pacific. In addition, there are two regions where TC genesis reaches maximum over the western North Pacific (Figure 2a). One is over the South China Sea (SCS) and the other one is on the east of Philippines. It seems that GPI_{ocean} mainly exhibits one peak over the SCS, which could be attributable to the lack of the atmospheric factors in GPI_{ocean}. For example, the relative humidity and vertical motion are not included in GPI_{ocean}, and both of them favor TC genesis over the Philippine Sea (Figures 4b and 4e will be discussed in detail later).

Although the oceanic factors and their formats in GPI_{ocean} are mainly determined by the statistical test and regression, the selections of $\bar{T}$ and D_{26} are physically understandable and are consistent with previous studies on physical mechanisms. For example, the impacts and dynamics of the subsurface environment on TC (although the TC intensity was mainly discussed, rather than TC genesis) have been extensively discussed in *Lin et al*. [2013], *Jin et al*. [2014], and *Huang et al*. [2015], in which the subsurface environment at a fixed depth (such as 80 m) was particularly examined. In fact, such depth can be either in the mixed layer or around D_{26}, depending on the locations. In addition, *Lin et al*. [2009] captured the increase of D_{26} and found that it was a major reason for the rapid increase of a typhoon. The relation between D_{26} and the development region of TCs was also discussed by *Pun et al*. [2013]. Note that not all previous studies focused on TC genesis. However, if the subsurface environment has impacts on the properties of TCs, it is reasonable to assume that it also has nonnegligible influences on their genesis. Thus, the relation between the subsurface

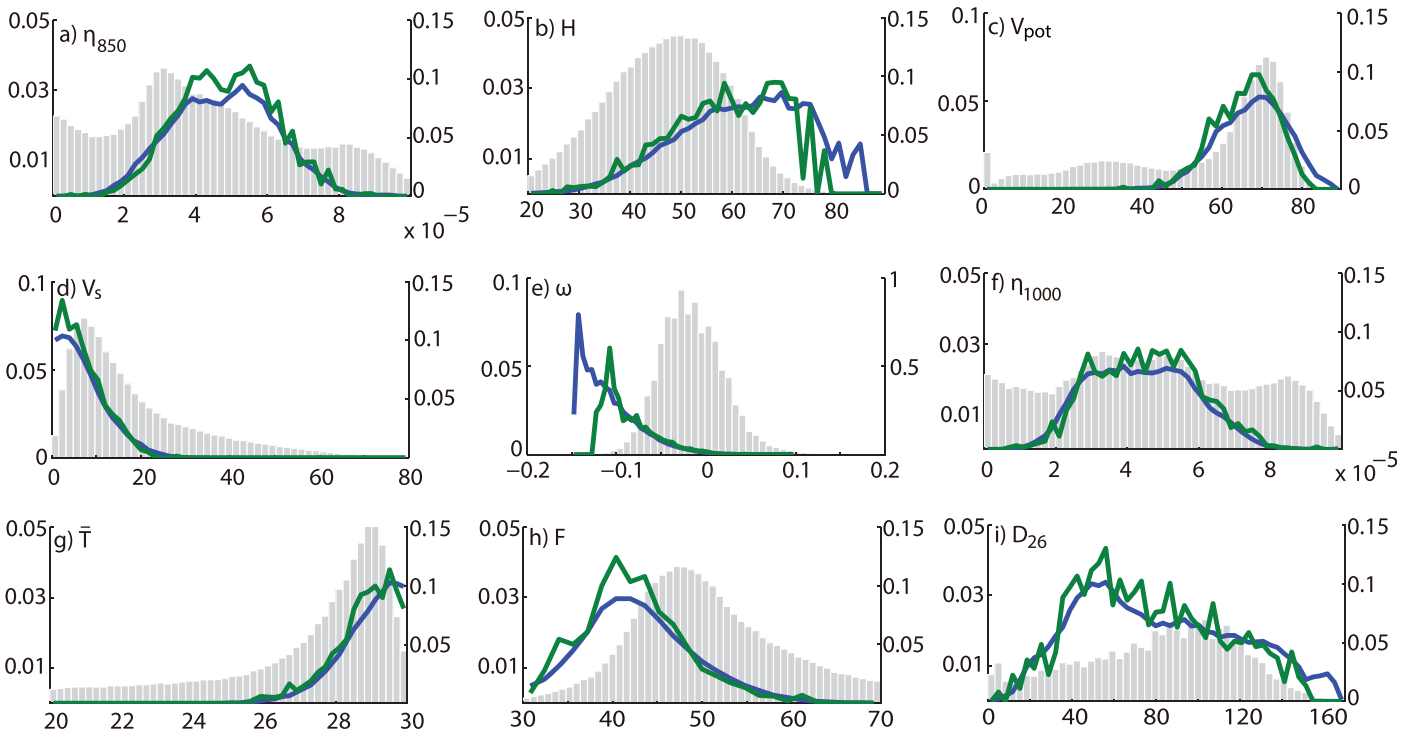

Figure 3. Green lines: Mean observed TC genesis number with respect to an individual factor (right axis). Blue lines: The marginal distributions of (a–e) $GPI10_{WP}$ and (f–i) GPI_{ocean} with respect to all factors (right axis) in equations (2) and (3). The marginal distributions are obtained by taking only one factor the interannual values but keeping all other factors the climatological values. Gay bars: Probability distribution of various factors (left axis). The unit for the left axis is percentage.

environment and TC genesis, which is indicated in GPI_{ocean} (equation (3)) is consistent with the physical understandings. One can also see the physical mechanisms behind the statistics from the marginal GPI distributions with respect to all factors in equations (2) and (3), as shown with blue lines in Figure 3. For each factor in a GPI, its marginal distribution is obtained by using the interannual value only for this factor, but keeping all other factors the climatological value. Meanwhile, the distributions of the observed TC genesis as a function of each factor are superimposed with green lines and the probability distributions of each factor over the western North Pacific are represented with gray bars.

The mean spatial distributions of all factors used in equations (2) and (3) from July to September are shown in Figure 4. As for $GPI10_{WP}$, most TCs generate when η_{850} is between 3×10^{-5} s^{-1} and 7×10^{-5} s^{-1} (the green line in Figure 3a), which generally occur between 10°N and 30°N (Figure 4a). In reality, this region indeed covers most TC genesis (Figure 2a). Thus, the dependence of TC genesis on η_{850} is captured by $GPI10_{WP}$ (blue line in Figure 3a). TC genesis increases with H until it reaches the maximum when H is around 70% (green line in Figure 3b). Higher H usually occurs to the south of 5°N (Figure 4b), which is too close to the equator for TC genesis. However, in equation (2), $GPI10_{WP}$ is proportional to H^b. As a result, the marginal $GPI10_{WP}$ is still large when H is larger than 70% (blue line in Figure 3b), leading to an obvious discrepancy. Nevertheless, for the whole $GPI10_{WP}$, such discrepancy is dismissed by other terms, such as η_{850}, which yields a very small marginal $GPI10_{WP}$ near the equator. In addition, the probability distribution of H centers around 50% (gray bars in Figure 3b) and only a small amount of H can reach 70%. Thus, as already known, the moistening of the lower troposphere (H is at 700 hPa in equation (2)) is a key factor for TC genesis. For V_{pot} and V_s, most TCs generate around 70 m s^{-1} and 5 m s^{-1}, respectively (green lines in Figure 3c and 3d). Such favorable conditions mainly occur in a zonal belt around 16°N (Figures 4c and 4d), which is consistent with TC genesis regions shown in Figure 2a. As a result, the probability distributions of V_{pot} and V_s (gray bars in Figures 3c and 3d) have a similar shape to the marginal distribution of TC genesis, and the blue lines and green lines are consistent with each other in Figures 3c and 3d. The vertical velocity ω is another key parameter in $GPI10_{WP}$, since the peak of gray bars and peak of green lines have a far distance. Moderate updraft (~ -0.05 Pa s^{-1}) occurs in some patches between the equator and 16°N (Figure 4e). However, the strong upward motion (~ -0.1 Pa s^{-1}) only happens sporadically and cannot be shown in the climatological

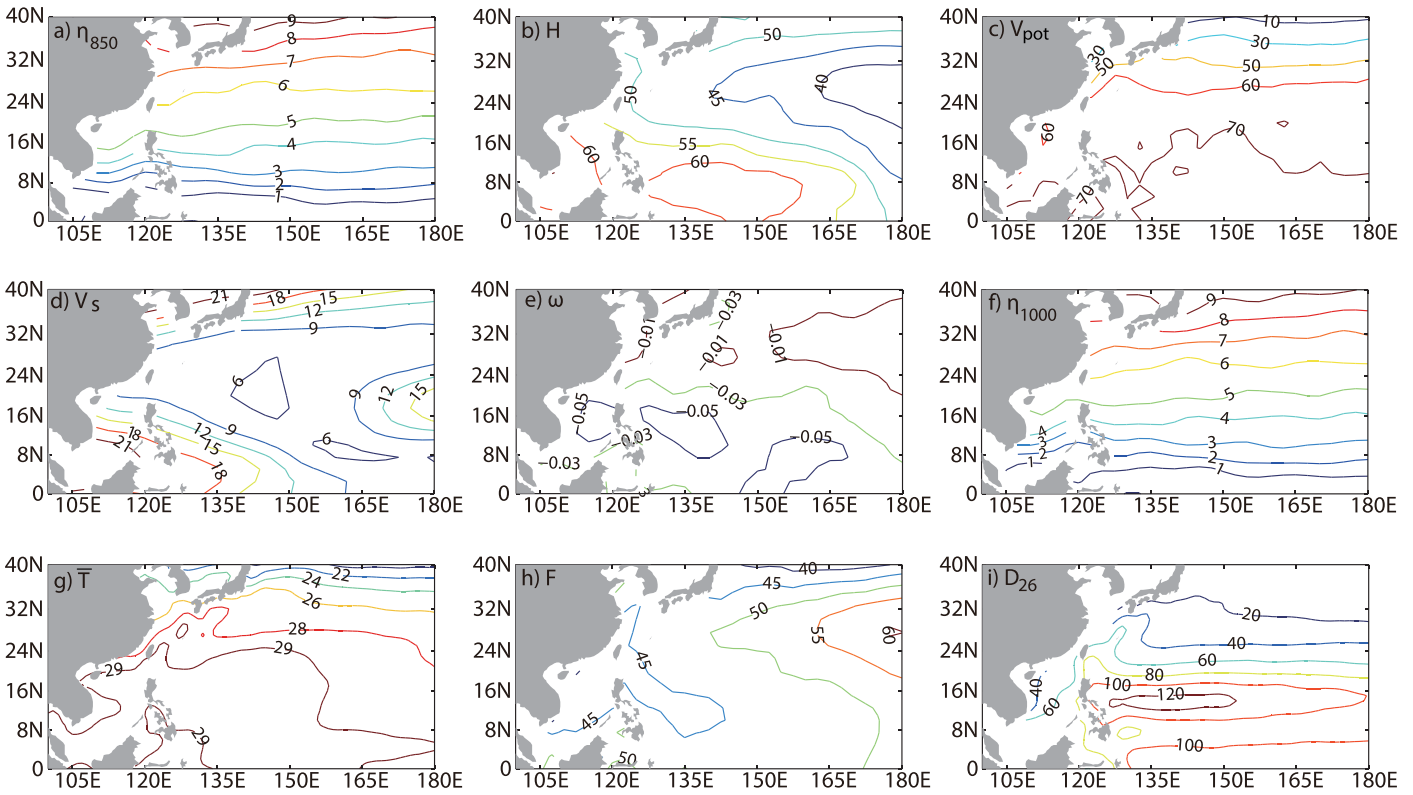

Figure 4. Climatological spatial distribution of different factors, averaged in July–September from 1948 to 2012. The contours in each panel are (a) η_{850} in $10^{-5}s^{-1}$; (b) H in percentage; (c) V_{pot} in m s^{-1}; (d) V_s in m s^{-1}; (e) ω in 10^{-2} Pa s^{-1}; (f) η_{1000} in $10^{-5}s^{-1}$; (g) $\bar{T}$ in °C; (h) F in W m^{-2}; (i) D_{26} in m.

contours in Figure 4e. $GPI10_{WP}$ captures the dependence of TC genesis on ω and reaches the maximum at a very strong vertical velocity (blue line in Figure 3e). As for GPI_{ocean}, its dependence on η_{1000} is very similar to the dependence of $GPI10_{WP}$ on η_{850} (Figures 3f and 4f). For the other three parameters in GPI_{ocean}, there is an obvious distance between the peak of their probability distributions (gray bars in Figures 3g–3i) and the peak of the marginal distributions of TC genesis (green lines in Figures 3g–3i), which implies that TC genesis is sensitive to these three factors. Large $\bar{T}$ occurs over the western Pacific warm pool and the northern SCS (Figure 4g) and GPI_{ocean} reproduces the shape of the marginal TC genesis distribution (blue line in Figure 3g). This is consistent with the conclusion in *Lin et al.* [2013] that $\bar{T}$ should be included in the GPI. However, high $\bar{T}$ extends northward along the Kuroshio, which explains the bias of GPI_{ocean} along the Kuroshio as shown in Figure 2f. Weak F ($<$50 W m^{-2}) also occurs over the western Pacific warm pool and the northern SCS (Figure 4h), so that the blue line follows the green line in Figure 3h. As shown in Figure 1i, there are two moderate peaks in the probability distribution of TC genesis with respect to D_{26}. However, in Figure 3i, there is only one peak between 40 and 60 m, corresponding to the shallow D_{26} over the SCS (Figure 4i). In contrast, D_{26} does not lead to frequent TC genesis over the western North Pacific. This is understandable, since TC genesis is likely to be sensitive to the warm water ($>$26°C) volume change where the warm water depth is shallow.

4. Seasonal and Interannual Properties of GPI_{ocean}

The major purpose and application of the empirical index for TC genesis is to facilitate the studies on the long-term TC variability. In this section, the new GPI with the oceanic parameters is shown to be capable of representing the seasonal and interannual variabilities of TC genesis. Especially, the GPI_{ocean} is shown to have the ability to capture the fingerprints of El Niño-Southern Oscillation (ENSO), which is the most important interannual pacemaker over the whole globe, on TC genesis.

The mean TC genesis numbers in each month (averaged from 1948 to 2012) are shown in Figure 5a (gray bars) along with the mean annual cycle of all GPIs. Over the western North Pacific, the TC genesis number is

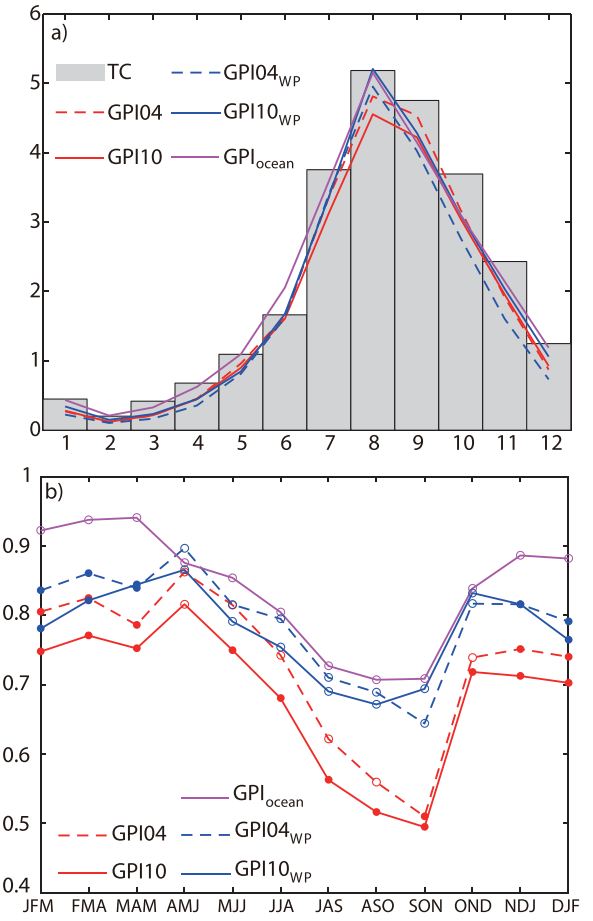

Figure 5. (a) Mean GPIs in each month, which are averaged from 1948 to 2012. The gray bars are the monthly mean TC genesis number obtained from JTWC. (b) Correlations between different GPIs and observations in every 3 months. The filled (open) circle indicates that the correlation between the GPI and observations is (is not) significantly different from the correlation between GPI_{ocean} and observations at a confidence level of 95%, using the Hotelling's *t* test. The statistical test results do not change if using the Steiger's *Z* test.

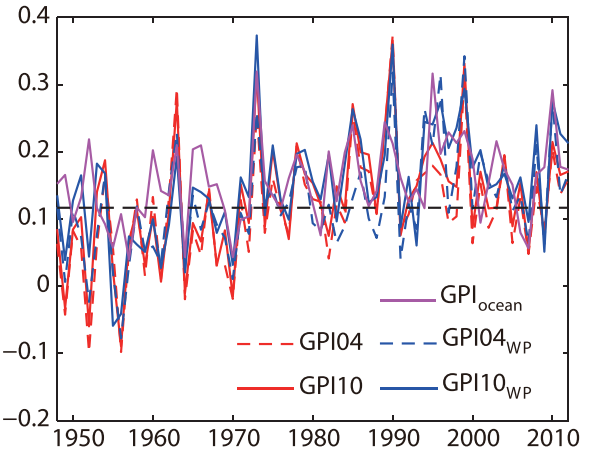

Figure 6. Spatial correlations between various GPIs and the observations in each year from 1948 to 2012. The black dash line marks a 95% confidence level.

large from July to November and decreases in other months. Such seasonal variability is well captured by all indices. Only GPI10 has slightly weak amplitude in boreal summer. Figure 5b shows the correlations between all GPIs and observations in every three months. Generally, all correlations are significant at a 95% confidence level, which indicates that all GPIs are able to capture the interannual variability of TC genesis. The correlations of GPI_{ocean} are slightly higher than those of $GPI04_{WP}$ and $GPI10_{WP}$, but most differences are not statistically significant (the open circles in Figure 5b). However, in boreal summer, the correlations between GPI_{ocean} and observations are significantly higher than those for GPI10 (the filled circles in Figure 5b). The GPIs show higher correlations with observations during boreal winter than they are in boreal summer, which is probably related to the spatial shift of TC associated with ENSO, as argued in *Camargo et al.* [2007a]. The spatial correlations between each GPI and the observations from 1948 to 2012 are shown in Figure 6. In most years, especially after the 1970s, the spatial correlations are statistically significant at a 95% confidence level. In addition, all GPIs show a very similar interannual variability. In addition, one can see the decadal variability in Figure 6. However, due to the limit of the data period, it is hard to draw a robust conclusion on the decadal variability and thus no detailed discussion is presented in this study.

Since TCs mainly generate in boreal summer in the Northern Hemisphere (Figure 3a), we only focus on JAS for the following analysis on the relation between TC genesis and ENSO. The El Niño and La Niña years are defined with the Nino3.4 index (area averaged SST anomalies from 5°S to 5°N and 170°E to 120°W) following *Trenberth* [1997]. An El Niño (La Niña) year is defined when the 5 month running mean Nino3.4 index is larger (smaller) than 0.4 (−0.4) for more than 6 months. The El Niño and La Niña years are listed in Table 4.

The observed TC genesis, $GPI10_{WP}$, and GPI_{ocean} in El Niño years, La Niña years, and their differences between the El Niño and the La Niña years are shown in Figure 7. Consistent with previous studies [e.g., *Chu*, 2004; *Wang and Chan*, 2002], TC genesis

Table 4. The El Niño Years and the La Niña Years Used for the Composites[a]

El Niño Years			La Niña Years			
1957	1987	1994	1950	1964	1975	1989
1972	1991	1997	1954	1971	1984	1999
1982	1992	2002	1955	1973	1985	2000
1983	1993	2009	1956	1974	1988	

[a]See the text for the detailed criteria.

locations move to the southeastern domain in the El Niño years (Box C in Figure 7f) and move to the northwestern domain in the La Niña years (Box A in Figure 7f), which is attributable to the eastward extension of the Pacific warm pool during El Niño years. However, $GPI10_{WP}$ yields a negative bias of TC genesis in the El Niño years in Box B (Figure 7f), which is removed in GPI_{ocean}. Following the same method in *Camargo et al.* [2007a], the importance of each variable is tested with the "individual perturbation", i.e., only one parameter in a GPI takes the interannual values and all other parameters are fixed to their climatology. This process is repeated for each factor in $GPI10_{WP}$ and in GPI_{ocean}, and the results are presented in Figures 8 and 9.

For $GPI10_{WP}$, the increase of TC genesis in the zonal belt around 15°N in the El Niño years is mainly attributable to the increase of η_{850}, which is consistent with *Camargo et al.* [2007a]. The influences of V_{pot} (Figure 8d) and V_s (Figure 8e) are modest. The relative humidity (Figure 8c) leads to a decrease of TC genesis over the northwestern domain in the El Niño years, which is due to the enhanced descending motion in this region. If the vertical velocity is not explicitly included, such as in GPI04, the decrease in TC genesis is mainly represented by the relative humidity. In contrast, when the vertical velocity is included (GPI10; Figure 8b), the decrease of TC genesis in the El Niño years is more represented by the vertical velocity. Meanwhile, the enhanced vertical velocity along 10°N is obvious, which also contributes to the increase of TC genesis in this region [*Wang and Chan*, 2002]. The negative bias in Box B in Figure 7f is attributable to ω (Figure 8b) and H (Figure 8c). In the El Niño years, due to the eastward shift of the convection center, ω and H are both reduced in Box B. However, the influence of such variation on TC genesis is overestimated by $GPI10_{WP}$.

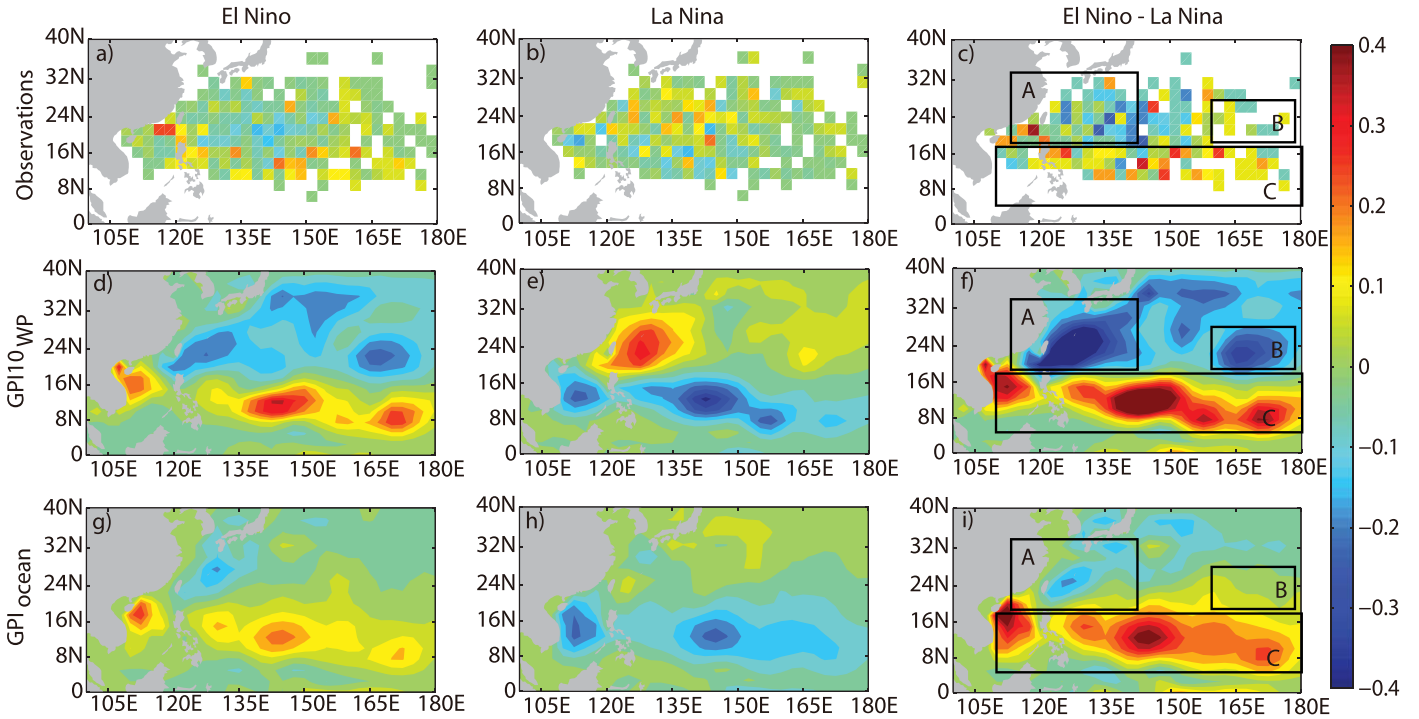

Figure 7. Differences in the mean TC genesis number between the El Niño years and the La Niña years (El Niño-La Niña). The first row is for the JTWC, the second row is for $GPI10_{WP}$, and the third row is for GPI_{ocean}. The first column is for the El Niño years, the second column is for the La Niña years, and the third column is for the differences between the El Niño years and the La Niña years. Boxes A–C mark three regions with pronounced differences.

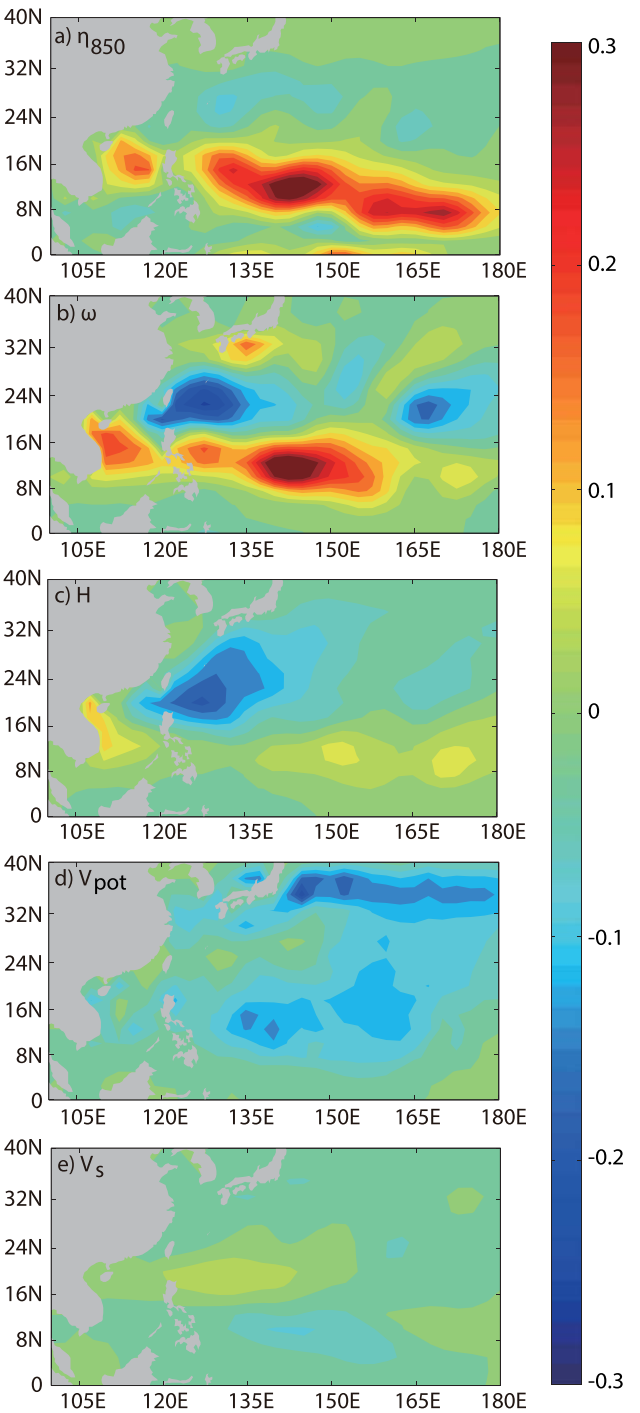

Figure 8. Differences of the mean $GPI10_{WP}$ between the El Niño years and the La Niña years (El Niño-La Niña) with interannual (a) η_{850}, (b) ω, (c) H, (d) V_{pot}, and (e) V_s. All other variables are fixed to their climatology.

The sensitivity of GPI_{ocean} to each factor in equation (3) is shown in Figure 9. The increase of TC genesis along 10°N and decease over the northwestern domain are also captured by GPI_{ocean} (Figure 7i). Similar to the effect of η_{850} in $GPI10_{WP}$, η_{1000} contributes to the increase of TC genesis during the El Niño years along the zonal belt around 15°N (Figure 9a). However, the amplitude of η_{1000} contribution is much smaller than that of η_{850}. Instead, the increase of TC genesis in the El Niño years is mainly attributable to F in GPI_{ocean} (Figure 9c). Note that since the exponent of F in equation (3) is negative, GPI_{ocean} is inversely proportional to F. Thus, negative F (upward F is defined positive) accompanies a large TC genesis number (Figure 9c), which is consistent with the fact that there is more total cloud cover over the western Pacific Ocean during the El Niño years than the La Niña years (Figure 10). During El Niño years, $\bar{T}$ decreases over the northwestern Pacific Ocean (Figure 9), which is favorable for the decrease of TC genesis (Box A in Figure 7i). Note that both observations and model simulations indicate that the local SST is not the only critical factor for TC genesis. Physically, the remote SST is also important for TC genesis, although it is not selected by the statistical regression process. $\bar{T}$ also decreases to the west of 140°E (especially over the SCS), which partly offsets the increase tendency of TC genesis due to F and η_{1000}. As a result, the increase of TC genesis to the west of 140°E is generally weaker than that to the east of 140°E. During the El Niño years, the warm water depth over the northwestern Pacific Ocean and the SCS becomes thinner than normal (not shown). As a result, TC genesis tends to decrease. However, the impact of D_{26} on the TC genesis is moderate compared with other three parameters in GPI_{ocean} (note that the color bar changes for Figure 9d), which is understandable because D_{26} denotes the subsurface processes in the ocean.

Generally, the differences in the GPIs between the El Niño and the La Niña years are the consequence of the changes in the ocean-atmosphere coupled system during the two climate states. Comparing Figures 7f and 7i, one can see that the differences between the El Niño years and the La Niña years in $GPI10_{WP}$ are generally stronger than those in GPI_{ocean} (Boxes A and C) and GPI_{ocean} is actually more consistent with the reality (Figure 7c). During the El Niño years, $\bar{T}$ in Box A decreases due to the eastward expansion of the

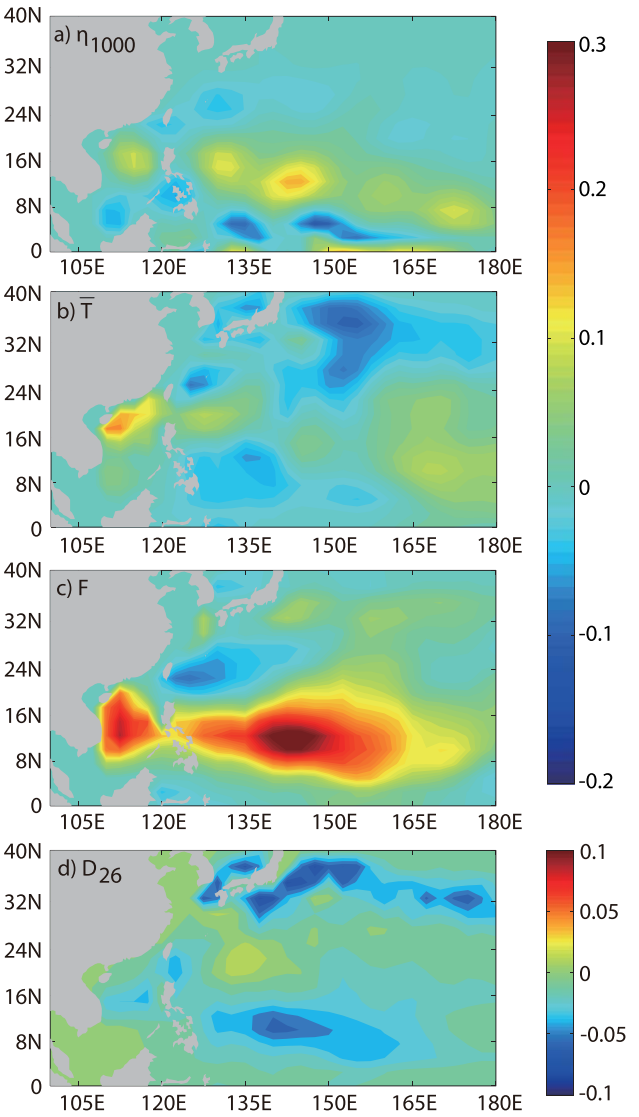

Figure 9. Differences of mean GPI_{ocean} between the El Niño years and the La Niña years (El Niño-La Niña) with interannual (a) η_{1000}, (b) $\bar{T}$, (c) F, and (d) D_{26}. All other variables are fixed to their climatology. Note that the color bar in Figure 9d is different from the color bars for other panels.

warm pool, which is consistent with the changes in SST. Correspondingly, ω and H reduce greatly over low $\bar{T}$, leading to stronger responses of $GPI10_{WP}$ than those of GPI_{ocean}. For Box C, all atmospheric factors in $GPI10_{WP}$ lead to an increase of the TC genesis in the El Niño years. The negative feedback comes from the PI, which incorporates the SST. By explicitly including the oceanic environment factors, the negative feedback from the ocean is better represented. As a result, the variability of TC genesis is better captured by GPI_{ocean}.

5. Conclusions and Discussion

A new TC genesis index (GPI_{ocean}), which adopts key oceanic factors, is has been proposed in this study. Various oceanic factors are chosen as candidate factors based on the physical understandings of the oceanic impacts on TCs. Then, regression and statistical tests are applied to select the factors that can significantly influence the performance of the new index. Note that a GPI cannot have a good performance if it only has oceanic factors. Thus, necessary atmospheric parameters at the sea surface are also included. Finally, GPI_{ocean} as defined in equation (3) is created. The components in GPI_{ocean} are not required to be independent from each other, since we only expect the index to have the best capture of the long-term variability of TC genesis. Comparing with existing GPIs, GPI_{ocean} is able to represent the climatology of TC genesis over the western North Pacific. It can also capture the seasonal and interannual variabilities of TC genesis. In general, GPI_{ocean} has a comparable effectiveness with $GPI10_{WP}$, which is the best index mainly using the atmospheric parameters. Although some physical mechanisms can be implied from GPI_{ocean}, GPI_{ocean} is not born from a theoretical framework, such as the theory of Carnot cycle for GPI04 [*Emanuel and Nolan*, 2004]. However, since there is still a lack of solid theory about the oceanic impacts on TC genesis, the statistical (though empirical) tool is useful for the studies on the long-term relation between the ocean and TCs. In addition, the statistical method is not supposed to select all oceanic variables that have a close physical connection with TC genesis. Instead, it intends to select a minimal subset of all possible

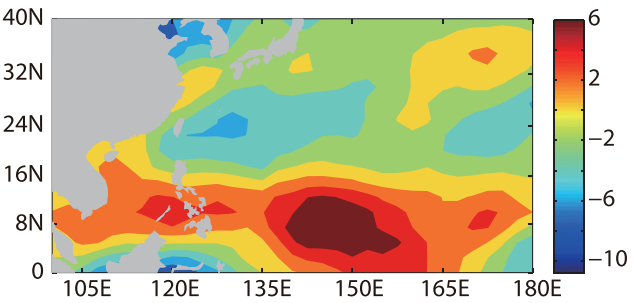

Figure 10. Differences in the total cloud cover between the El Niño years and the La Niña years (El Niño-La Niña). The unit is %.

parameters and enables the best performance of the GPI. For example, much evidence has shown that remote SST plays an important role in TC activities. This factor is listed as a candidate in this study. Although it is not selected by the stepwise regression process, it does not imply any inconsistency with our physical understanding.

In this study, our motivation is to explicitly include the oceanic parameters (especially the parameters about subsurface oceanic environment) in a GPI, so that the relation between the oceanic processes and the long-term variability of TC genesis can be quantitatively studied. In the context of climate change, the warming at the ocean subsurface becomes a hot topic [e.g., *Meehl et al*., 2011; *England et al*., 2014; *Johansson et al*., 2015; *Roberts et al*., 2015, and many others] and the impact of such variability on the long-term TC variability is of great interest. GPI_{ocean} provides a quantitative tool which connects the subsurface oceanic environment and the long-term variability of TC genesis. It can be used for such studies with oceanic reanalysis products and ocean climate model outputs, which cannot be done with existing GPIs since they do not explicitly adopt enough oceanic parameters. Thus, it will be helpful to obtain a more comprehensive understanding of the TC tendency under climate change. Note that, using the statistical method, the causality between the subsurface environment and the slow variability of TC genesis cannot be fully determined. It is just demonstrated that the subsurface environment (such as D_{26}) has a statistically significant relation with TC genesis, and it is useful for reproducing TC genesis with the GPI. The physical mechanisms of the oceanic impacts on TC genesis require further and devoted studies. When choosing the necessary atmospheric parameters, we select the ones at the sea surface on purpose, because such atmospheric parameters (such as the surface winds which are used to obtain the surface absolute vorticity) are necessary to be given as forcing terms for an ocean GCM and they are usually available. Therefore, the inclusion of the sea surface parameters does not ruin the possible application of GPI_{ocean}.

We do not intend to argue that the atmospheric parameters are not important in TC genesis. Actually, if the stepwise regression process is repeated by using all atmospheric and oceanic properties as candidates, we obtain the GPI as:

$$GPI_{atm_ocean} = p|10^5\eta_{850}|^{1.2}\left(\frac{-\omega+0.1}{0.1}\right)^{1.8}\left(\frac{LH}{100}\right)^{-0.6}\left(\frac{\bar{T}}{26}\right)^{10}\left(\frac{D_{26}}{80}\right)^{0.13}, \quad (4)$$

where LH denotes the latent heat flux and all other parameters carry the same meanings as defined above, $p = 1.5 \times 10^{-2}$. The climatological mean GPI_{atm_ocean} is shown in Figure 2g, which is very similar to that of GPI_{ocean}. The correlation between GPI_{atm_ocean} and the observations is 0.58, which is not significantly higher than the correlation between GPI_{ocean} and observations (which is 0.54 as shown in Table 2). Since GPI_{atm_ocean} and GPI_{ocean} have comparable abilities to represent the long-term variabilities of TC genesis, a comprehensive evaluation of GPI_{atm_ocean} is not presented. It is actually more reasonable to use η_{850} in a GPI. But, note that the index using η_{850} (GPI_{atm_ocean} in equation (4)) and the index using η_{1000} (GPI_{Ocean} in equation (3)) do not have significant difference in representing TC genesis over the western North Pacific. GPI_{ocean} is one of the indices that has the best performance of capturing TC genesis over the western North Pacific. Ocean GCM outputs and ocean reanalysis products usually do not have winds at 850 hPa. However, since the sea surface winds (i.e., winds near 1000 hPa) are always available, it will be convenient to use η_{1000}, instead of η_{850}, and their performance in the index will not be significantly different.

The research domain is limited to the western North Pacific, which can make our results more reliable. Nevertheless, the techniques used in this study can be applied to any ocean basin. For example, the whole statistical processes are applied to the whole globe and another GPI (GPI_{globe}) is obtained (not shown). However, the fitness between GPI_{globe} and the observations in every ocean basin is low and the performance of GPI_{globe} over the western North Pacific is much worse than GPI_{ocean}, because TC genesis in different ocean basin is likely to have different statistical properties. By analogy, for GPI04 and GPI10, the format of the index remains the same, but the coefficients can change over the western North Pacific (Table 2). In addition, *Fu et al*. [2012] and *Peng et al*. [2012] found that the key parameters for TC genesis are different between the western North Pacific and the North Atlantic, indicating that a uniform GPI formula at a global scale may not be suitable for each basin. Therefore, the dependence of TC genesis on the oceanic factors and their statistical relations can change from one ocean basin to another. Of course, it is straightforward to apply the statistical processes used in this study to other ocean basins.

Acknowledgments
The authors thank the anonymous reviewers for their insightful comments and suggestions that have contributed to improve this paper. All data for this paper are properly cited and referred to in the reference list. This work was supported by National Basic Research Program of China (2013CB430302 and 2013CB430301), National Science Foundation of China (41376034 and 41321004), National Program on Global Change and Air-Sea Interaction (GASI-IPOVAI-02, GASI-IPOVAI-01-02, and GASI-IPOVAI-04), and Fundamental Research Funds for the Central Universities (2014B30514).

References

Ballabrera-Poy, J., R. Murtugudde, and A. J. Busalacchi (2002), On the potential impact of sea surface salinity observations on ENSO predictions, *J. Geophys. Res.*, *107*(C12), 8007, doi:10.1029/2001JC000834.

Black, P. G., E. A. D'asaro, W. M. Drennan, J. R. French, P. P. Niiler, T. B. Sanford, E. J. Terrill, E. J. Walsh, and J. A. Zhang (2007), Air-sea exchange in hurricanes—Synthesis of observations from the coupled boundary layer air-sea transfer experiment, *Bull. Am. Meteorol. Soc.*, *88*, 357–374.

Bruyère, C. L., G. J. Holland, and E. Towler (2012), Investigating the use of a genesis potential index for Tropical Cyclones in the North Atlantic Basin, *J. Clim.*, *25*, 8611–8626.

Camargo, S. J., K. A. Emanuel, and A. H. Sobel (2007a), Use of a genesis potential index to diagnose ENSO effects on tropical cyclone genesis, *J. Clim.*, *20*, 4819–4834.

Camargo, S. J., A. H. Sobel, A. G. Barnston, and K. A. Emanuel (2007b), Tropical cyclone genesis potential index in climate models, *Tellus, Ser. A*, *59*, 428–443.

Chan, J. C. L., and K. S. Liu (2004), Global warming and western North Pacific typhoon activity from an observational perspective, *J. Clim.*, 17, 4590–4602.

Chu, P.-S. (2004), *ENSO and tropical cyclone activity*. Hurricanes and Typhoons: Past, Present, and Future, Columbia University Press, 297–332.

Chu, P. C., Q. Liu, Y. Jia, and C. Fan (2002), Evidence of a barrier layer in the Sulu and Celebes Seas, *J. Phys. Oceanogr.*, *32*, 3299–3309.

Chu, P. C., C. W. Fan, and C. Sun (2010), Changes of heat and freshwater contents in the world ocean mixed layer (1990–2009) identified from in situ and Argo measurements, in 42nd International Liege Colloquium on Ocean Dynamics, Liege, Belgium, April 26–30.

de Boyer Montégut, C., G. Madec, A. S. Fischer, A. Lazar, and D. Iudicone (2004), Mixed layer depth over the global ocean: An examination of profile data and a profile-based climatology, *J. Geophys. Res.*, *109*, C12003, doi:10.1029/2004JC002378.

Defant, A. (1961), *Physical Oceanography*, vol. 2, Pergamon Press, N. Y.

Draper, N. R., and H. Smith (1998), *Applied Regression Analysis*, pp. 327–368, John Wiley, N. Y.

Emanuel, K. (2005), Increasing destructiveness of tropical cyclones over the past 30 years, *Nature*, *436*, 686–688.

Emanuel, K. A. (1995), Sensitivity of tropical cyclones to surface exchange coefficients and a revised steady-state model incorporating eye dynamics, *J. Atmos. Sci.*, *52*, 3969–3976.

Emanuel, K. A. (1997), Some aspects of Hurricane inner-core dynamics and energetics, *J. Atmos. Sci.*, *54*, 1014–1026.

Emanuel, K. A. (2010) Tropical cyclone activity downscaled from NOAA-CIRES reanalysis, 1908–1958, *J. Adv. Model. Earth Syst.*, *2*, 1–12.

Emanuel, K. A., and D. Nolan (2004), Tropical cyclone activity and the global climate system, preprints, 26th Conference on Hurricanes and Tropical Meteorology, Miami, Fla., Am. Meteor. Soc. A.

England, M. H., S. McGregor, P. Spence, G. A. Meehl, A. Timmermann, W. Cai, A. S. Gupta, M. J. McPhaden, A. Purich, and A. Santoso (2014), Recent intensification of wind-driven circulation in the Pacific and the ongoing warming hiatus, *Nat. Clim. Change*, *4*, 222–227.

Fu, B., M. S. Peng, T. Li, and D. E. Stevens (2012), Developing versus nondeveloping disturbances in the North Atlantic and Western North Pacific. Part II: The Western North Pacific, *Mon. Weather Rev.*, *140*, 1067–1080.

Good, S. A., M. J. Martin, and N. A. Rayner (2013), EN4: Quality controlled ocean temperature and salinity profiles and monthly objective analyses with uncertainty estimates, *J. Geophys. Res. Oceans*, *118*, 6704–6716, doi:10.1002/2013JC009067.

Gray, W. M. (1979), Hurricanes: Their formation, structure and likely role in the tropical circulation, *Meteorol. Tropical Oceans*, *77*, 155–218.

Hotelling, H. (1940), The selection of variates for use in prediction with some comments on the general problem of nuisance parameters, *Ann. Math. Stat.*, *11*, 271–283.

Huang, P., I. I. Lin, C. Chou, and R.-H. Huang (2015), Change in ocean subsurface environment to suppress tropical cyclone intensification under global warming, *Nat Commun.*, *6*, 7188.

Jin, F. F., J. Boucharel, and I. I. Lin (2014), Eastern Pacific tropical cyclones intensified by El Nino delivery of subsurface ocean heat, *Nature*, *516*, 82–85.

Johansson, D. J. A., B. C. O'Neill, C. Tebaldi, and O. Haggstrom (2015), Equilibrium climate sensitivity in light of observations over the warming hiatus, *Nat. Clim. Change*, *5*, 449–453.

Kalnay, E., et al. (1996), The NCEP/NCAR 40-year reanalysis project, *Bull. Am. Meteorol. Soc.*, *77*, 437–471.

Kara, A. B., P. A. Rochford, and H. E. Hurlburt (2000), Mixed layer depth variability and barrier layer formation over the North Pacific Ocean, *J. Geophys. Res.*, *105*, 16,783–16,801.

Kara, A. B., R. W. Helber, T. P. Boyer, and J. B. Elsner (2009), Mixed layer depth in the Aegean, Marmara, Black and Azov Seas. Part I: General features, *J. Mar. Syst.*, *78*, S169–S180.

Lamb, P. (1984), On the mixed-layer climatology of the north and tropical Atlantic, *Tellus, Ser. A*, *36*, 292–305.

Lin, I. I., C.-H. Chen, I.-F. Pun, W. T. Liu, and C.-C. Wu (2009), Warm ocean anomaly, air sea fluxes, and the rapid intensification of tropical cyclone Nargis (2008), *Geophys. Res. Lett.*, *36*, L03817, doi:10.1029/2008GL035815.

Lin, I. I., P. Black, J. F. Price, C.-Y. Yang, S. S. Chen, C.-C. Lien, P. Harr, N.-H. Chi, C.-C. Wu, and E. A. D'Asaro (2013), An ocean coupling potential intensity index for tropical cyclones, *Geophys. Res. Lett.*, *40*, 1878–1882, doi:10.1002/grl.50091.

Lukas, R., and E. Lindstrom (1991), The mixed layer of the western equatorial Pacific Ocean, *J. Geophys. Res.*, *96*, 3343–3357.

Meehl, G. A., J. M. Arblaster, J. T. Fasullo, A. Hu, and K. E. Trenberth (2011), Model-based evidence of deep-ocean heat uptake during surface-temperature hiatus periods, *Nat. Clim. Change*, *1*, 360–364.

Menkes, C. E., M. Lengaigne, P. Marchesiello, N. C. Jourdain, E. M. Vincent, J. Lefevre, F. Chauvin, and J. F. Royer (2011), Comparison of tropical cyclogenesis indices on seasonal to interannual timescales, *Clim. Dyn.*, *38*, 301–321.

Murakami, H., and B. Wang (2010), Future change of North Atlantic Tropical Cyclone tracks: Projection by a 20-km-mesh global atmospheric model, *J. Clim.*, *23*, 2699–2721.

Park, J. J., Y.-O. Kwon, and J. F. Price (2011), Argo array observation of ocean heat content changes induced by tropical cyclones in the north Pacific, *J. Geophys. Res.*, *116*, C12025, doi:10.1029/2011JC007165.

Peng, M. S., B. Fu, T. Li, and D. E. Stevens (2012), Developing versus nondeveloping disturbances in the North Atlantic and Western North Pacific. Part I: The North Atlantic, *Mon. Weather Rev.*, *140*, 1047–1066.

Price, J. F. (2009), Metrics of hurricane-ocean interaction: Vertically-integrated or vertically-averaged ocean temperature?, *Ocean Sci.*, *5*, 351–368.

Pun, I.-F., I. I. Lin, and M.-H. Lo (2013), Recent increase in high tropical cyclone heat potential area in the Western North Pacific Ocean, *Geophys. Res. Lett.*, *40*, 4680–4684, doi:10.1002/grl.50548.

Rao, R. R., R. L. Molinari, and J. F. Festa (1989), Evolution of the climatological near-surface thermal structure of the tropical Indian Ocean: 1. Description of mean monthly mixed layer depth, and sea surface temperature, surface current, and surface meteorological fields, *J. Geophys. Res.*, *94*, 10,801–10,815.

Rayner, N. A., D. E. Parker, E. B. Horton, C. K. Folland, L. V. Alexander, D. P. Rowell, E. C. Kent, and A. Kaplan (2003), Global analyses of sea surface temperature, sea ice, and night marine air temperature since the late nineteenth century, *J. Geophys. Res.*, *108*(D14), 4407, doi: 10.1029/2002JD002670.

Roberts, C. D., M. D. Palmer, D. McNeall, and M. Collins (2015), Quantifying the likelihood of a continued hiatus in global warming, *Nat. Clim. Change*, *5*, 337–342.

Royer, J. F., F. Chauvin, B. Timbal, P. Araspin, and D. Grimal (1998), A GCM study of the impact of greenhouse gas increase on the frequency of occurrence of tropical cyclones, *Clim. Change*, *38*, 307–343.

Scoccimarro, E., S. Gualdi, A. Bellucci, A. Sanna, P. Fogli, E. Manzini, M. Vichi, P. Oddo, and A. Navarra (2011), Effects of tropical cyclones on ocean heat transport in a high-resolution coupled general circulation model, *J. Clim.*, *24*, 4368–4384.

Shay, L. K., G. J. Goni, and P. G. Black (2000), Effects of a warm oceanic feature on hurricane opal, *Mon. Weather Rev.*, *128*, 1366–1383.

Silva, M., M. Araujo, J. Servain, P. Penven, and C. A. Lentini (2009), High-resolution regional ocean dynamics simulation in the southwestern tropical Atlantic, *Ocean Modell.*, *30*, 256–269.

Sprintall, J., and D. Roemmich (1999), Characterizing the structure of the surface layer in the Pacific Ocean, *J. Geophys. Res.*, *104*, 23,297–23,311.

Steiger, J. H. (1980), Tests for comparing elements of a correlation matrix, *Psychol. Bull.*, *87*, 245–251.

Thompson, R. O. (1976), Climatological numerical models of the surface mixed layer of the ocean, *J. Phys. Oceanogr.*, *6*, 496–503.

Tippett, M. K., S. J. Camargo, and A. H. Sobel (2011), A poisson regression index for tropical cyclone genesis and the role of large-scale vorticity in genesis, *J. Clim.*, *24*, 2335–2357.

Trenberth, K. E. (1997), The definition of El Niño, *Bull. Am. Meteorol. Soc.*, *78*, 2771–2777.

Uppala, S. M., et al. (2005), The ERA-40 re-analysis, *Q. J. R. Meteorol. Soc.*, *131*, 2961–3012.

Vecchi, G. A., and B. J. Soden (2007a), Effect of remote sea surface temperature change on tropical cyclone potential intensity, *Nature*, *450*, 1066–1070.

Vecchi, G. A., and B. J. Soden (2007b), Increased tropical Atlantic wind shear in model projections of global warming, *Geophys. Res. Lett.*, *34*, L08702, doi:10.1029/2006GL028905.

Vincent, E., M. Lengaigne, C. Menkes, N. Jourdain, P. Marchesiello, and G. Madec (2011), Interannual variability of the South Pacific Convergence Zone and implications for tropical cyclone genesis, *Clim. Dyn.*, *36*, 1881–1896.

Wang, B., and J. C. L. Chan (2002), How strong ENSO events affect tropical storm activity over the Western North Pacific, *J. Clim.*, *15*, 1643–1658.

Wang, C., and L. Wu (2016), Interannual shift of the tropical upper-tropospheric trough and its influence on tropical cyclone formation over the western North Pacific, *J. Clim.*, *29*, 4203–4211.

Wu, C.-C., C.-Y. Lee, and I. I. Lin (2007), The effect of the ocean eddy on tropical cyclone intensity, *J. Atmos. Sci.*, *64*, 3562–3578.

Wu, L., C. Wang, and B. Wang (2015), Westward shift of western North Pacific tropicalcyclogenesis, *Geophys. Res. Lett.*, *42*, 1537–1542.

Yokoi, S., Y. Takayabu, and J. L. Chan (2009), Tropical cyclone genesis frequency over the western North Pacific simulated in medium-resolution coupled general circulation models, *Clim. Dyn.*, *33*, 665–683.

Yu, J., C. Chen, T. Li, X. Zhao, H. Xue, and Q. Sun (2016), Contribution of major SSTA modes to the climate variability of tropical cyclone genesis frequency over the western North Pacific, *Q. J. R. Meteorol. Soc.*, *142*, 1171–1181.

Zhang, W., G. Vecchi, H. Murakami, G. Villarini, and L. Jia (2016), The Pacific meridional mode and the occurrence of tropical cyclones in the western North Pacific, *J. Clim.*, *29*, 381–398.

Zhao, M., and I. M. Held (2012), TC-permitting GCM simulations of hurricane frequency response to sea surface temperature anomalies projected for the late-twenty-first century, *J. Clim.*, *25*, 2995–3009.